A lightweight fault diagnosis model for planetary gearbox using domain adaptation and model compression

Mengmeng Song[1], Zicheng Xiong[2], Zexiong Zhang[3], Jihua Ren[4], Mengwei Li[5], Shungen Xiao[6], Yaohong Tang[7]
[1, 6, 7]College of Information, Mechanical and Electrical Engineering, Ningde Normal University, Ningde 352000, China
[2]College of Mechanical Engineering and Automation, Fuzhou University, Fuzhou 350000, China
[3, 5]College of Mechanical and Electrical Engineering, Fujian Agriculture and Forestry University, Fuzhou 350000, China
[4]Dongguan Xinghuo Gear Co., Ltd, Dongguan 523000, China
[6]Corresponding author
E-mail: [1]*544824964@qq.com*, [2]*2814210225@qq.com*, [3]*1963414543@qq.com*, [4]*sharyren@xhgear.com*, [5]*1620200241@qq.com*, [6]*xiaoshungen022@163.com*, [7]*264572049@qq.com*

Received 22 May 2023; accepted 3 October 2023; published online 23 January 2024
DOI https://doi.org/10.21595/jve.2023.23412

Abstract. This article proposes a novel lightweight attention spatiotemporal joint distribution adaptation network fault diagnosis model to address the key challenges of domain transfer and high model complexity in traditional methods. The novelty lies in 1. Using model compression techniques to reduce the complexity of the network model and improve its computational efficiency; 2. Introducing new domain adaptation and adversarial methods to solve the domain transfer problem. The effectiveness of the proposed model is verified through a transfer experiment of planetary gearbox vibration data. The experimental results show that the proposed model reduces the parameters and computational complexity to 18 % and 15 % of the original model, respectively, and has a diagnostic accuracy of over 98 % in cross-condition transfer tasks, and still maintains an accuracy of over 88 % even under high noise levels. This indicates that the proposed model is an efficient and accurate fault diagnosis model.

Keywords: transfer learning, fault diagnosis, attention mechanism, model compression technology.

1. Introduction

Bearing, gear and other rotating mechanical parts are the parts with the highest failure rate in mechanical equipment. Timely fault diagnosis of rotating mechanical parts can ensure the safe and stable operation of mechanical equipment and avoid economic losses caused by failures.

The traditional mechanical fault diagnosis method mainly consists of two steps: artificial feature extraction and artificial pattern recognition. That is, first, manually extract the feature map that is easier to distinguish the fault type from the acoustic, optical, vibration acceleration, temperature and other signals, and then directly judge the fault type through the feature map. However, the method relying on artificial feature extraction is only applicable to situations where the complexity of the mechanical system dynamics model is low. In the case of high complexity, the features that can significantly represent the health state of the machine cannot be obtained, so it is not conducive to pattern recognition. In addition, in the case of high system complexity, the results of pattern recognition are easy to be affected by the subjective cognitive bias of experts, resulting in reduced accuracy of pattern recognition. The emergence of the machine learning (ML) method solves the problem of relying on artificial pattern recognition. After establishing the discrimination model, this method trains the parameters of the model through a large number of labeled data, so that the model can output the fault discrimination results, thus avoiding the risk of accuracy decline caused by subjective judgment. Fault diagnosis models based on traditional ML include support vector machine, decision tree, K nearest neighbor algorithm, etc. Li et al. [1] used a multi-core support vector machine to diagnose the fault of a gas turbine and verified the performance of the model through comparative experiments. For the structure of the model itself and the problem of computational efficiency, some scholars solve it by simplifying the model parameters and improving the algorithm for optimizing the model. For example, Vong et al. [2] extract features through wavelet packet transform. With the extracted features, the engine faults are then classified by a multi-class least squares support vector machine. Li et al. [3] used particle swarm optimization to improve the training process of SVM.

With the development of ML technology in recent years, intelligent fault diagnosis has also come into being. Among them, intelligent fault diagnosis based on deep learning (DL) solves the problem that the feature extraction of traditional machine fault diagnosis depends on the prior knowledge of experts. The DL model can automatically extract more complete fault features for classification. To lower the model's complexity, many scholars first use traditional feature transformation to extract shallow features from the original data, and then use DL technology to extract deep-level features and conduct pattern recognition [4]. Fault diagnosis methods based on DL often use convolutional neural networks [5] (CNN), recurrent neural networks [6] (RNN), generative adversarial networks [7] (GAN), deep belief networks [8] (DBN), stacked autoencoders [9] (SAE) and other models. Islam et al. [4] collected the signal of the bearing through the acoustic transmitter, converted the information into wavelet spectrum by wavelet packet transform, then selected the band signal with significant characteristics through the defect rate index, and finally input the band signal into the adaptive CNN to diagnose the fault. Demetgul et al. [10] used Diffusion Maps, Local Linear Embedding, and AutoEncoders for feature extraction, and used Gustafson-Kessel and k-medoids algorithms to classify encoded signals, achieving good diagnostic accuracy in fault diagnosis of material handling systems. Zhang et al. [11] supplement-ed the original data set through Gan to make the sample categories balanced, and then used CNN model for feature extraction and pattern recognition. Through comparative experiments, it was proved that the fault diagnosis effect of this approach is better than that of the approach without data expansion. Zhao et al. [12] proposed a deep branch attention network, which can flexibly integrate vibration and velocity information to obtain higher diagnostic accuracy.

The premise of the application of the above fault diagnosis method is that the training samples and the test samples are independent and identically distributed in the probability distribution. However, in the actual situation, the probability distribution of the machine state data is often different due to different working conditions. The distribution difference between training data and test data will cause a domain confrontation phenomenon [13], which will greatly reduce the model diagnosis accuracy. Therefore, it is necessary to introduce domain adaptation into fault diagnosis methods to solve the problem of domain offset. In many industrial contexts, it is challenging to collect labeled data for practical applications, while it is simpler to collect non-labeled data. Based on this, this paper will realize the mapping of the original data to the machine health state under variable conditions through unsupervised deep domain adaptive transfer learning (TL) method, that is, build an end-to-end model, and train the model through labeled source domain data and unlabeled target domain data. TL-based intelligent fault methods have received a lot of attention recently. Te et al. [14] used convolutional neural networks as feature extractors and classifiers, and added domain classifiers to the model. Through confrontation training, the feature extractors can extract common features of the two domains, and finally conduct fault diagnosis through the classifier. Xu et al. [15] obtained the simulation fault data of the workshop through the data twin technology, and then realized the fault diagnosis of the actual workshop through the simulation fault data and the improved sparse stacking automatic encoder.

The general approximation theorem points out that a multilayer feedforward network containing enough hidden layer neurons can approximate any continuous function with any accuracy. However, the development direction of DL model is always towards the trend of more layers and larger width scales. Due to the limitation of hardware on computing power, the number of hidden layer neurons and network layers will be limited, while simply increasing the network depth of the model will increase the risk of gradient cliff or gradient explosion. At the same time, the computational efficiency of the huge model is low, which is not conducive to real-time fault diagnosis. In order to enhance the capability of feature extraction and pattern discrimination under limited model parameters, it is necessary to optimize the model parameters and computational complexity. The technology of model compression and accelerated depth neural network has been continuously developed in recent years, and is widely used to reduce the parameter amount and calculation amount of the model. This technology can be divided into parameter pruning and quantization, low-rank decomposition, transfer/compact convolution filter and knowledge distillation [16]. For the traditional DL-based fault diagnosis technology, there are problems of accuracy drop caused by domain offset and redundancy of model parameters and computation.

This paper aims at the problem of domain confrontation and the redundancy of model parameters and computation in the DL fault diagnosis method. This paper proposes a spatio-temporal neural network (STN) based on convolutional neural network (CNN) and long short memory network (LSTM). On the basis of STN, attention mechanism (AM) is introduced to enhance the significance of extracted features. Then domain adaptation and domain confrontation mechanism are introduced to strengthen the robustness of fault diagnosis under different working conditions. Finally, a lightweight attention spatio-temporal network fusion joint distribution domain adaptation (AST-JDAN) fault diagnosis model is obtained through model compression technology.

2. Theoretical background

2.1. Soft attention mechanism

The purpose of AM is to enable each feature vector to obtain the similarity between features, so that similar features can obtain more significant feature interaction, and finally enable the model to extract more significant fault features to promote fault diagnosis.

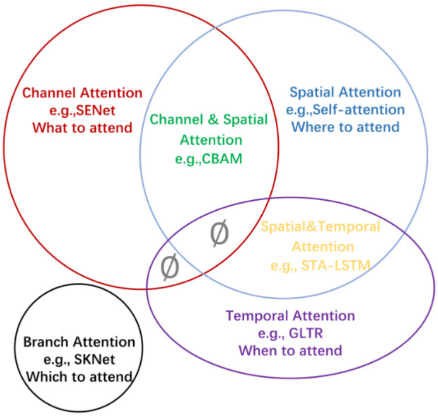

Fig. 1. Wayne diagram of AM classification [17]

The AM can be broken down into channel attention, space attention, time attention, space-time attention, space channel attention, and branch attention, as shown in Fig. 1. This paper mainly deals with spatial AM. Spatial AM is divided into soft AM and hard AM according to the weight of selected fault eigenvalue. The soft AM takes each feature into account, and the weight of each feature is between 0 and 1, while the hard AM only selects the features that have a large relationship. The weight of the features that have a large relationship is 1, and the weight of the features that have a small relationship is 0. Because the hard AM excludes the features of small relationship, it may lead to information omission and affect the fault diagnosis accuracy of the model, so this paper selects the soft AM.

As shown in Fig. 2, the hard AM is like an addressing process, which finds the value stored in the address space through a fixed address, while the soft AM is similar to the soft addressing process. The difference from the hard AM is that each time the query vector matches a key value pair, v will be output, and the proportion of the output depends on the degree of correlation between the query vector and the key vector. In the hard AM, it is believed that each time the key value pair is matched, it is either 100 % related or irrelevant.

The output features through the soft AM are mainly divided into the following steps: (1) Prepare the query vector q, the key vector k, and the value vector v. In this fault diagnosis model, q is the feature of the last time step of LSTM layer output in STN, k and v are the output of each time step of LSTM and the output of each channel of convolution layer. (2) Calculate the score s (also called attention distribution) of each characteristic v, and weight v output. The calculation formula of s is shown in Eq. (1):

$$s_i = p(z = i|K, q) = Softmax\big(score(k_i, q)\big), \quad i = 1,2,\ldots,N. \tag{1}$$

Among them, $score$ is a $score$ function to calculate the degree of correlation between the key vector and the query vector. The score function usually uses the dot product model, as shown in Eq. (2), that is, the dot product between vectors is calculated to represent the correlation between vectors. Obviously, when two vectors are orthogonal (independent), the scoring value is 0. The scaling point product model is shown in Eq. (3), which reduces $d^{1/2}$ based on the point product model, where d is the dimension of input k_i. Eq. (4) is a bilinear model, which introduces a trainable weight matrix W on the basis of the point product model. The author Kim [18], who proposed the model, believes that the conventional point product model establishes a separate attention distribution for each category, ignoring the correlation between multiple categories of inputs. By introducing W, the knowledge of attention distribution established by each category will be learned by W, making contributions to the establishment of attention distribution of the next category. Wu [19] proposed an additive model, as shown in Eq. (5). Compared with the bilinear model, it increases the attention value U_q of A global context awareness and is activated through the $\tanh$ function. Where, W and U are trainable weight matrices:

$$score(x_i, q) = x_i^T q, \tag{2}$$
$$score(x_i, q) = \frac{x_i^T q}{\sqrt{d}}, \tag{3}$$
$$score(x_i, q) = x_i^T W q, \tag{4}$$
$$score(x_i, q) = v^T \tanh(W x_i + U q). \tag{5}$$

After obtaining the attention distribution s, let $k = v$, and obtain the output value of the AM lay er through weighted summation, as shown in Eq. (6):

$$att(X, q) = \sum_{i=1}^{N} s_i v_i = \sum_{i=1}^{N} s_i k_i. \tag{6}$$

2.2. Domain countermeasure mechanism

Ganin et al. [20] introduced the domain confrontation learning mechanism in the deep neural network in 2016, and proposed the domain adversarial neural network (DANN). DANN consists of three networks, including feature extractor (G_f), classifier (G_y) and domain discriminator (G_d). The function of feature extractor is to extract the features of source domain and target domain;

The function of the classifier is to classify features; The function of the domain discriminator is to distinguish whether the features produced by the feature extractor come from source domain data or target domain data as much as possible.

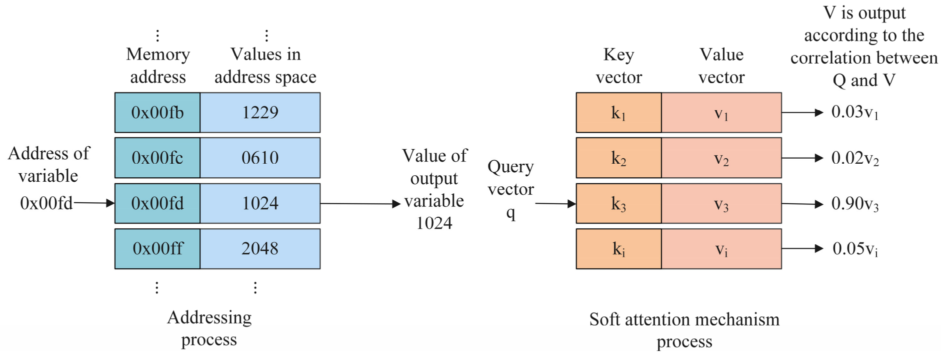

Fig. 2. Comparison of addressing process and soft AM process

The training goal of DANN is to enable the classifier to accurately classify the source domain features and make the domain discriminator unable to distinguish whether the features produced by the feature extractor come from the source domain data or the target domain data. In this way, the source domain and target domain can be mapped to the same feature space, the distribution between the two domains can be aligned, and then the target domain data can be classified through a classifier. The objective function expression of confrontation training is shown in Eq. (7):

$$\min_{y}\max_{d} L(y,d) = \sum_{i=1}^{N} L_y\left(G_y\left(G_f\left(x_i;\theta_f\right);\theta_y\right),y_i\right) + \sum_{i=1}^{N} L_d\left(G_d\left(R_\lambda\left(G_f\left(x_i;\theta_f\right)\right);\theta_d\right),d_i\right), \quad (7)$$

where, N is the number of samples, x_i is the input sample, y_i is the sample label, d_i is the domain label, θ_f, θ_y and θ_d is the weight matrix of G_f, G_y and G_d respectively, L_y is the cross entropy loss function of class discrimination, L_d is the cross entropy loss function of domain discrimination, R_λ is a gradient inversion layer function, which keeps the independent variable output during feedforward propagation unchanged, while the gradient of the independent variable during backpropagation becomes the original -λ times.

2.3. Model compression technology

The enormous model's poor computational efficiency makes it difficult to diagnose faults in real time, necessitating the optimization of model parameters and computing. The DL model compression theory has been developed recently.

MobileNet [21] proposed by Google is an efficient model compression algorithm. Its core innovation is to replace the original convolution layer with depth separable convolution, which can achieve the same pattern recognition effect as the original model while reducing the number of model parameters and calculations. Depth separable convolution decomposes ordinary convolution operations into channel by channel convolution (DW) and point by point convolution (PW) [22]. The calculation process of ordinary convolution and depth separable convolution is shown in Fig. 3.

The upper part of Fig. 3 is a general convolution process. Each filter consists of several convolution cores. The quantity of channels in the output feature is the same as the quantity of filters. The parameter quantities (params) and calculation quantities (FLOPs) of the general convolution are shown in Eq. (8) and Eq. (9):

$$params = C_i \cdot k_w \cdot k_h \cdot C_o, \tag{8}$$

$$FLOPs = C_o \cdot f_w \cdot f_h \cdot C_i \cdot k_w \cdot k_h, \tag{9}$$

where C_o is the number of filters, C_i is the number of convolution kernels for each filter, k_w is the width of the convolution kernel, k_h is the height of the convolution kernel, f_w is the width of the output feature map, and f_h is the height of the output feature map.

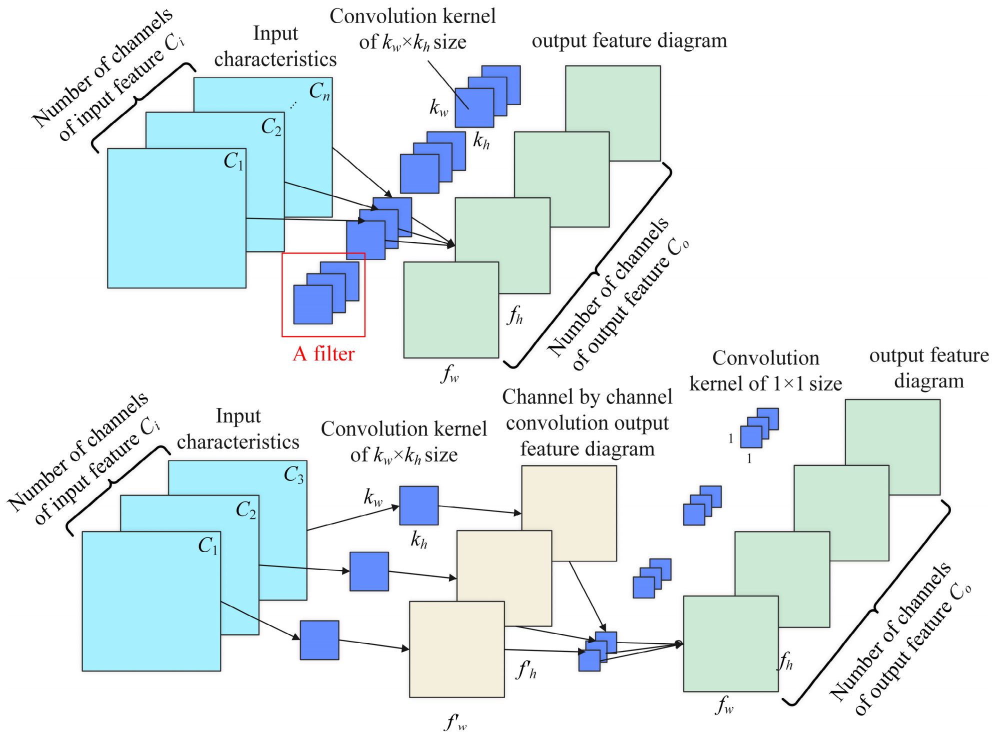
Number of channels of input feature C_i
Input characteristics
Convolution kernel of k_w×k_h size
output feature diagram
C_n
C_2
C_1
k_w
k_h
A filter
f_h
f_w
Number of channels of output feature C_o
Number of channels of input feature C_i
Input characteristics
C_3
C_2
C_1
Convolution kernel of k_w×k_h size
k_w
k_h
Channel by channel convolution output feature diagram
f'_h
f'_w
Convolution kernel of 1×1 size
1
1
output feature diagram
f_h
f_w
Number of channels of output feature C_o

Fig. 3. Comparison between ordinary convolution and deep separable convolution

The depth separable convolution integrates the ordinary convolution into two stages, first channel by channel convolution (DW), and then point by point convolution (PW). In DW, $C_i = 1$, $k_w = 1$, $k_h = 1$, and other parameters of ordinary convolution are the same. Combining Eq. (8), Eq. (9) and adding the parameter quantities and calculation quantities of DW and PW respectively, we can get the parameter quantities and calculation quantity formulas of depth separable convolution:

$$params = C_i \cdot k_w \cdot k_h \cdot 1 + C_i \cdot 1 \cdot 1 \cdot C_o = C_i \cdot (k_w \cdot k_h + C_o), \tag{10}$$

$$FLOPs = 1 \cdot f_w \cdot f_h \cdot C_i \cdot k_w \cdot k_h + C_o \cdot f_w \cdot f_h \cdot C_i \cdot 1 \cdot 1 = f_w \cdot f_h \cdot C_i \cdot (k_w \cdot k_h + C_o). \tag{11}$$

GhostNet [23] proposed by Huawei Noah Lab is also one of the efficient compression model algorithms. It replaces the feature map generated by the original part of the convolution through an operation that saves the number of parameters and computation, thereby saving hardware resources. The feature map is called the ghost feature map. The process of generating the phantom feature map is shown in Fig. 4.

If the number of channels generated by the low-cost operation is C_p, the phantom feature map matrix generated by each channel can be represented by Eq. (12):

$$(f_{op})_j = \varphi_j(f_i), \quad i = 1,2,\dots,C_p, \quad j = 1,2,3,\dots,C_o - C_p\,, \tag{12}$$

where, f_i is the feature map generated by ordinary convolution of the ith sheet. If ordinary convolution is used to generate the feature map of C_p sheet, j low-cost operations are performed φ_j Generate C_o-C_p phantom feature map f_{op}. In order to save computing resources, it is required that $C_o - C_p \geq C_p$.

In this paper, packet convolution is selected as a low-cost operation, and the schematic diagram of packet convolution is shown in Fig. 5. Grouped convolution divides the channels of the input feature into g groups, and the number of convolution cores of the filter is the same as the number of channels of the input feature C_i. Therefore, each filter should also divide the convolution cores into g groups, and each group should perform convolution operations separately. Finally, all the feature maps output by the filter are spliced according to the channel dimensions. The formula for the number of parameters and calculation amount is shown in Eq. (13) and Eq. (14):

$$params = \left(\frac{C_i}{g} \cdot k_w \cdot k_h\right) \cdot \frac{C_o}{g} \cdot g = \frac{C_i \cdot k_w \cdot k_h \cdot C_o}{g}, \tag{13}$$

$$FLOPs = \left(\frac{C_o}{g} \cdot f_w \cdot f_h\right) \cdot \left(\frac{C_i}{g} \cdot k_w \cdot k_h\right) \cdot g = \frac{C_o \cdot f_w \cdot f_h \cdot C_i \cdot k_w \cdot k_h}{g}. \tag{14}$$

It can be seen from Eq. (13) and Eq. (14) that the parameter amount and calculation amount of the packet convolution are $1/g$ of the ordinary convolution. It can be seen that the packet convolution is a cheaper operation than the ordinary convolution.

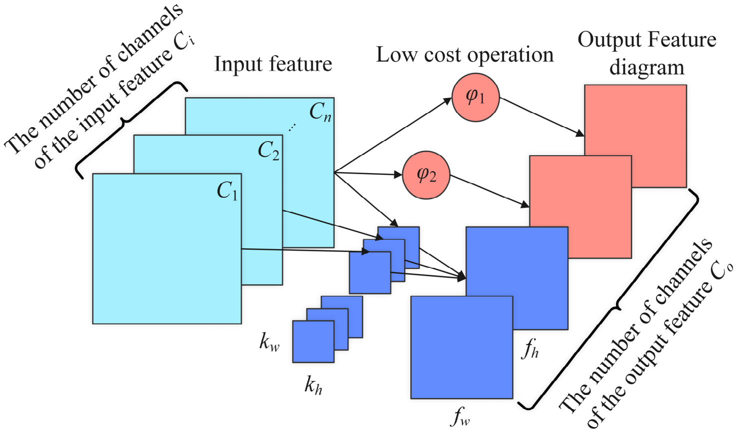

Fig. 4. Convolution diagram of GhostNet

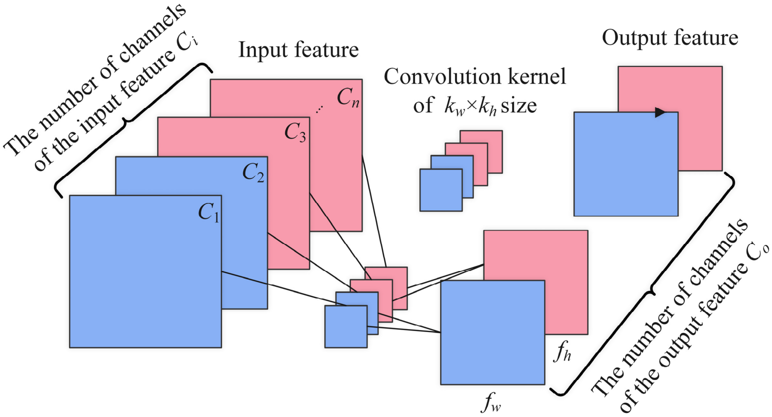
The number of channels of the input feature C_i
Input feature
Convolution kernel of $k_w \times k_h$ size
Output feature
C_n
C_3
C_2
C_1
f_h
f_w
The number of channels of the output feature C_o

Fig. 5. Schematic diagram of grouping convolution

2.4. Fusion domain adaptive fault diagnosis model based on lightweight spatio-temporal attention network

First, the soft AM is introduced into the end of the feature generator of the spatio-temporal neural network based on feature transfer learning (ST-JAN) [24], so that the network model can extract more significant fault features. Secondly, the domain confrontation mechanism is introduced to further migrate, so that the diagnosis model has better cross domain fault diagnosis capability. Finally, the model compression technology in MobileNet and GhostNet is introduced to reduce the parameter amount and calculation amount of the convolution layer in the diagnostic model and improve the calculation efficiency. Fig. 6 shows the architecture of AST-JDAN. The parameter settings of AST-JDAN are shown in Table 1.

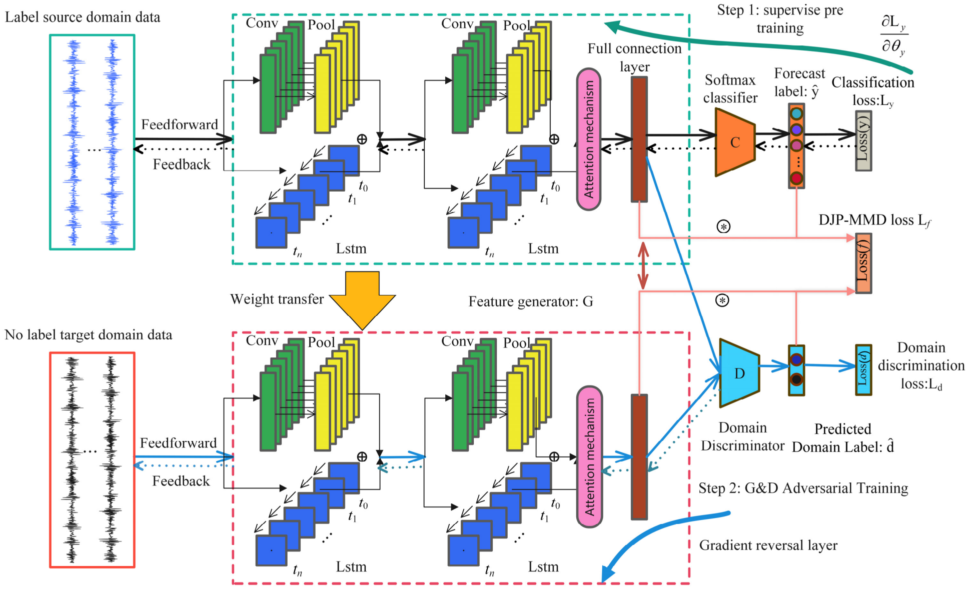

Fig. 6. Fusion domain adaptive fault diagnosis model based on spatio-temporal attention network

Table 1. Model parameters of ASTN-JDAN.

Network layer type		Kernel size	Number of hidden units	Step size	Output tensor shape
ASTN feature generator	Input	*	*	*	(N,1,1024)
	Conv1d(1)	64	*	1	(N,16,963)
	BatchNorm1d(1)	*	*	*	(N,16,963)
	MaxPool1d(1)	3	*	2	(N,16,482)
	LSTM(1)	64	482	*	(N,16,482)
	Conv1d(2)	3	*	1	(N,32,482)
	BatchNorm1d (2)	*	*	*	(N,32,482)
	AdaptiveMaxPool1d	*	*	*	(N,32,30)
	LSTM(2)	15	30	*	(N,32,30)
	Attention mechanism layer	*	256	*	(N,256)
Fault category discriminator	Linear(1)	*	256	*	(N,256)
	Linear(2)	*	128	*	(N,256)
	Fault classifier	*	10	*	(N,10)
Domain discriminator	Gradient reversal layer	*	*	*	(N,256)
	Linear(3)	*	256	*	(N,256)
	Linear(4)	*	256	*	(N,128)
	Linear(5)	*	2	*	(N,2)

According to the relevant formula in Section 2.3, the parameter quantity and calculation quantity of the original convolution layer, as well as the parameter quantity and calculation quantity of the convolution layer after model compression can be calculated. Table 2 presents the outcomes. It can be seen from Table 2 that the parameters of the improved convolution layer are compressed from the original 2560 to 464, about 18 % of the original, while the calculated FLOPs are compressed from the original 1726464 to 262128, about 15 % of the original.

Table 2. Comparison of parameters of convolutional layers after model compression

Convolutional layer	Ordinary convolution 1	Ordinary convolution 2	Depthwise separable convolution 1	Grouped convolution 2
Number of input channels C_i	1	16	1	16
Convolution kernel size $k_w * k_h$	1*64	3	1*64	3
Number of output channels C_o	16	32	16	32
Output feature Size $f_w * f_h$	1*963	1*482	1*963	1*482
Parameter quantity params	1024	1536	80	384
Amount of computation FLOPs	986112	740352	77040	185088
Total amount of parameters	2560		464	
Total calculation amount	1726464		262128	

3. Fault diagnosis test of secondary planetary gearbox

3.1. Introduction to DDS experimental platform

The experimental data comes from the vibration signals of the secondary planetary gearbox collected on the Drivetrain Diagnostics Simulator (DDS) test bench, as shown in Fig. 7. The test-bed can simulate the wear, crack, broken tooth and missing tooth faults of straight and helical gears, as well as the faults of inner ring, outer ring and rolling element of rolling bearings. Different working conditions can be simulated by setting different speeds and loading different torsional loads. DDS test bench is mainly composed of power module, spindle module and brake. In the power module, the variable speed drive motor provides power. The speed control panel controls the motor speed. The torque sensor and encoder are used to collect the torque and detect the pulse signal generated by the speed. The real-time display displays the actual speed. Because of the slip and other factors in gear transmission, the set speed is often slightly lower than the actual speed. The main shaft module mainly includes the main shaft, parallel gearbox and secondary planetary gearbox. In addition, an acceleration sensor is installed on the gearbox to collect fault vibration signals. The programmable magnetic powder brake at the end of the test bench is used to control the load of the spindle and simulate the rotation under different loads.

In this experiment, the fault gear of the secondary planetary gearbox is set on the sun gear, and there are four fault types in total, namely, missing tooth, broken tooth, surface wear and tooth root crack, as shown in Fig. 8. In addition, the gear is normal, and there are five health conditions for the gear.

3.2. Test data collection

The sampling frequency set in the experiment is 12.8 kHz. The motor has two rotation frequencies of 20 Hz and 30 Hz, and the load current size is 0.4 A and 0.8 A. Therefore, the experiment has four working conditions: 20 Hz 0.4 A, 20 Hz 0.8 A, 30 Hz 0.4 A and 30 Hz 0.8 A. The four working conditions are named as A, B, C and D. Each working condition has five health conditions of gears: normal, missing, broken, surface wear and tooth root crack. Through the statistics of each original data file, it can be found that the number of samples of each type under each working condition is consistent, and the data volume is sufficient, reaching 1048548 data points, without data imbalance. Therefore, sufficient samples can be directly collected by non-overlapping sampling, that is, the sampling step is equal to the sample length $n = 1024$. The expression of the total sample size M is shown in Eq. (15), where the constant 5 represents the data of five machine health states, and $l = 1048548$ is the length of each type of data. The total sample size under each working condition is obtained by Eq. (15), as shown in Table 3:

$$M = 5 \times \left\lfloor \frac{l}{n} \right\rfloor. \tag{15}$$

Table 3. Data length and sampling quantity of DDS test bench planetary gearbox under each working condition

No.	Working condition	Health condition	Data size	Sample size	Total sample size
A	20 Hz 0.4 A	Normal	1048548	1023	5115
		Missing teeth	1048548	1023	
		Broken teeth	1048548	1023	
		Surface wear	1048548	1023	
		Root crack	1048548	1023	
B	20 Hz 0.8 A	Normal	1048548	1023	5115
		Missing teeth	1048548	1023	
		Broken teeth	1048548	1023	
		Surface wear	1048548	1023	
		Root crack	1048548	1023	
C	30 Hz 0.4 A	Normal	1048548	1023	5115
		Missing teeth	1048548	1023	
		Broken teeth	1048548	1023	
		Surface wear	1048548	1023	
		Root crack	1048548	1023	
D	30 Hz 0.8 A	Normal	1048548	1023	5115
		Missing teeth	1048548	1023	
		Broken teeth	1048548	1023	
		Surface wear	1048548	1023	
		Root crack	1048548	1023	

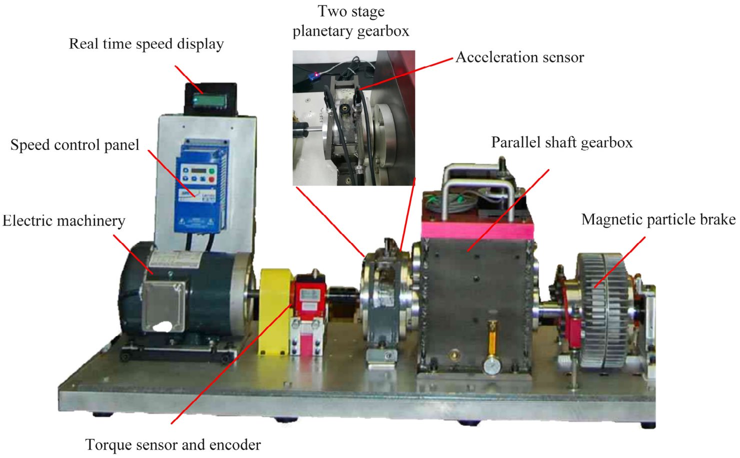

Fig. 7. Drivetrain diagnostics simulator test bench

Fig. 9 shows two samples of CWRU fault bearing data set and DDS planetary gearbox data set. The blue part of Fig. 9(a) and Fig. 9(b) is the original vibration signal, and the red part is the envelope of the original vibration signal. Then, the envelope spectrum of the signal is obtained through the envelope line of fast Fourier transform, as shown in Fig. 9(c) and Fig. 9(d). It is not difficult to find that the sideband spectrum of the planetary gearbox is more complex from the spectrum diagram, which indicates that the fault diagnosis of the planetary gearbox signal of the DDS test bench is more difficult. This is a greater challenge for the transfer task of the model.

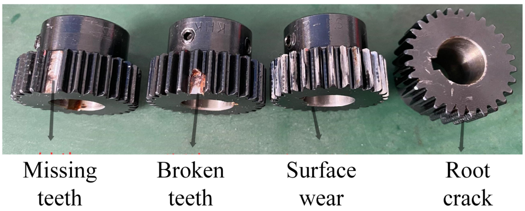

Fig. 8. Machining simulation of four kinds of gear faults

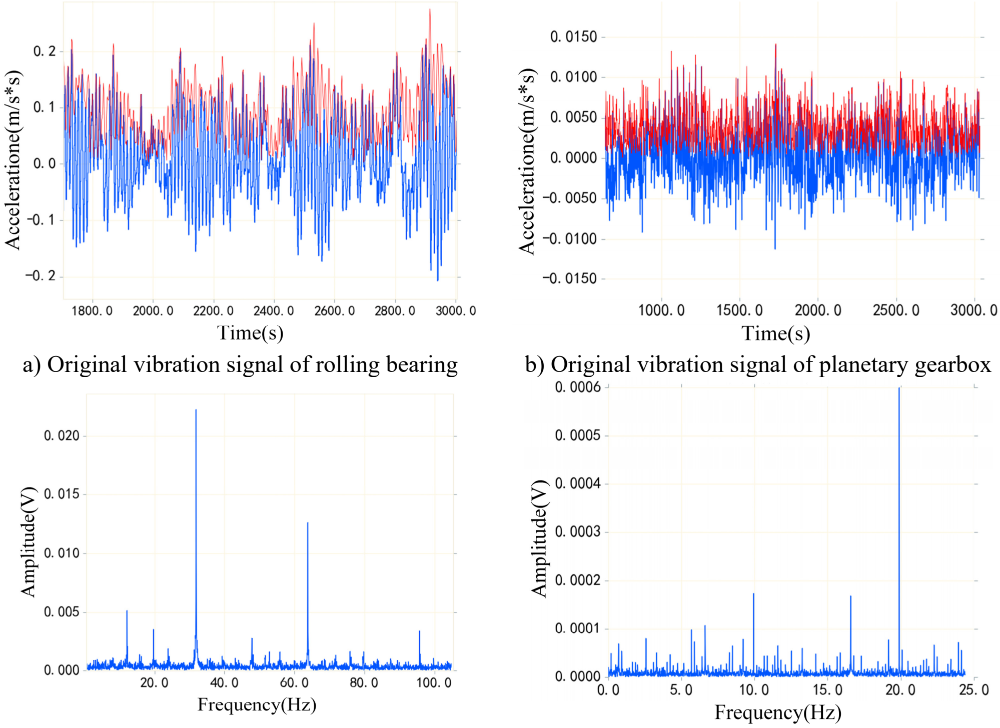

a) Original vibration signal of rolling bearing

b) Original vibration signal of planetary gearbox

c) Rolling bearing envelope spectrum

d) Planetary gearbox envelope spectrum

Fig. 9. Comparison of envelope spectra of bearing data and planetary gearbox data

3.3. The influence of attention mechanism

The AM introduced earlier can adaptively screen out the favorable features for machine fault diagnosis tasks. Therefore, in the soft AM, each part can be given different weights as the realization form of soft screening. The model used in this section is AST-JDAN fault diagnosis model. The working condition of source domain data is 20 Hz 0.4 A, and that of target domain data is 20 Hz 0.8 A. The AST-JDAN model is trained with source domain data, and then the attention weight distribution of different health state data is extracted from it, as shown in Fig. 10. The distribution of attention weight can reflect the degree of attention paid to different time steps.

It can be seen from Fig. 10 that data in different health states have significantly different attention distribution rules. For tooth breakage fault, the attention distribution is mainly concentrated on the later time step, and slightly concentrated in the middle, which is similar to the attention distribution of surface wear fault, but the latter distribution is more concentrated on the later time step, and the weight value in the middle is smaller. The attention distribution of missing teeth fault and gear normal is close to the forward time step, but the attention distribution of gear normal is more concentrated on the left side, and the weight value in the middle is smaller; The attention of the crack fault is concentrated in the middle of the time step, and gradually decreases at both ends.

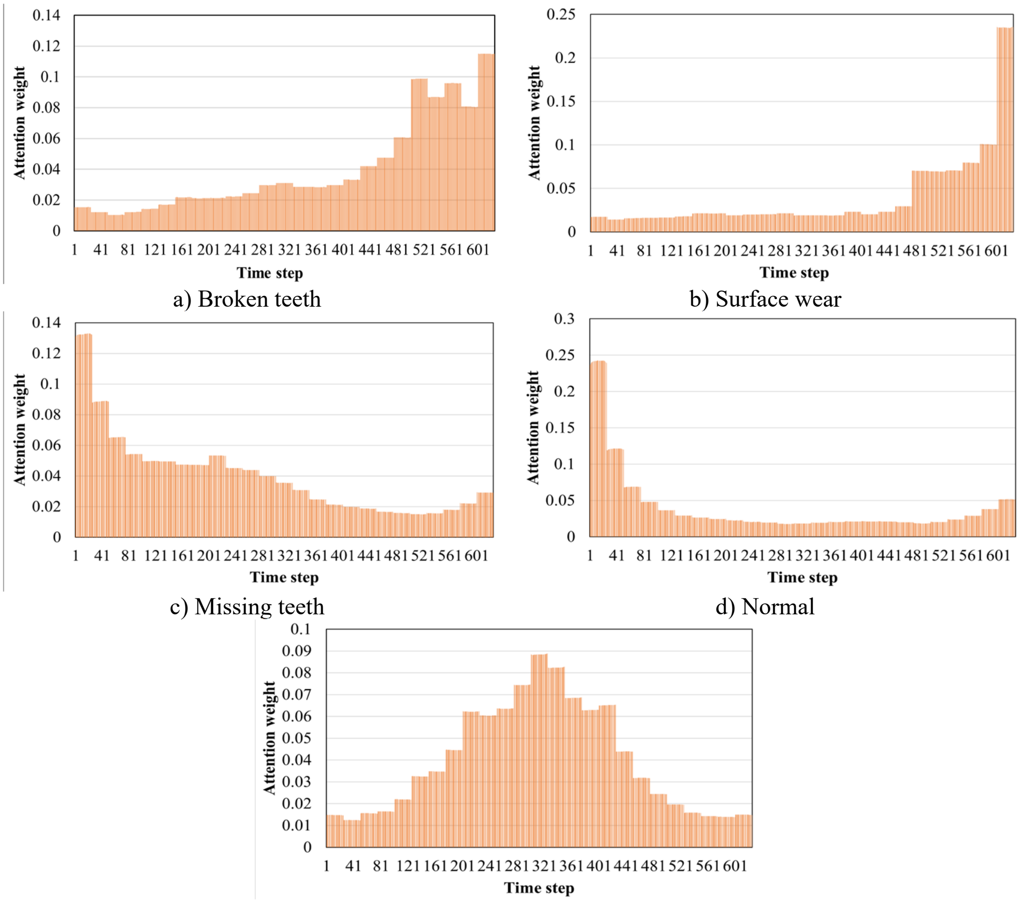

a) Broken teeth

b) Surface wear

c) Missing teeth

d) Normal

e) Root crack

Fig. 10. Attention distribution diagram of different sun wheel health states

In order to reveal the influence of attention distribution in the transfer process, the source domain and target domain are input into the trained AST-JDAN model, and the extracted attention distribution is shown in Fig. 11. The yellow line represents the attention weight distribution diagram of the source domain data, and the blue line represents the attention weight distribution diagram of the target domain data. It can be seen from Fig. 11 that data with the same health status in different domains have generally similar attention weight distribution, which enables the AM in the target domain to enhance the features conducive to pattern recognition.

In order to explore the influence of AM layer on pattern recognition, the target field tooth break fault data and crack fault data are input to the trained AST-JDAN, and their output features are spliced and visualized through channels. The results are shown in Fig. 12. It can be seen from Fig. 12 that the output characteristics of two different fault category data before the AM layer are similar, showing similar periodic pulses. Through careful observation, it can be seen that the activation value of the feature output of the broken tooth fault shows a trend of gradually decreasing on both sides of the middle high, similar to a spindle. However, the crack fault shows a tendency for the two sides of the middle concave bulge first and then decrease. This small difference is difficult for the classifier to classify. After the AM layer, the characteristics of the middle part of the tooth fracture data are enhanced, while the characteristics of the two sides are relatively weakened, making the overall shape of the features more easily distinguishable. At the same time, the characteristics of the two peaks of the crack fault are also more significantly changed, which verifies the ability of the AM to enhance the data characteristics.

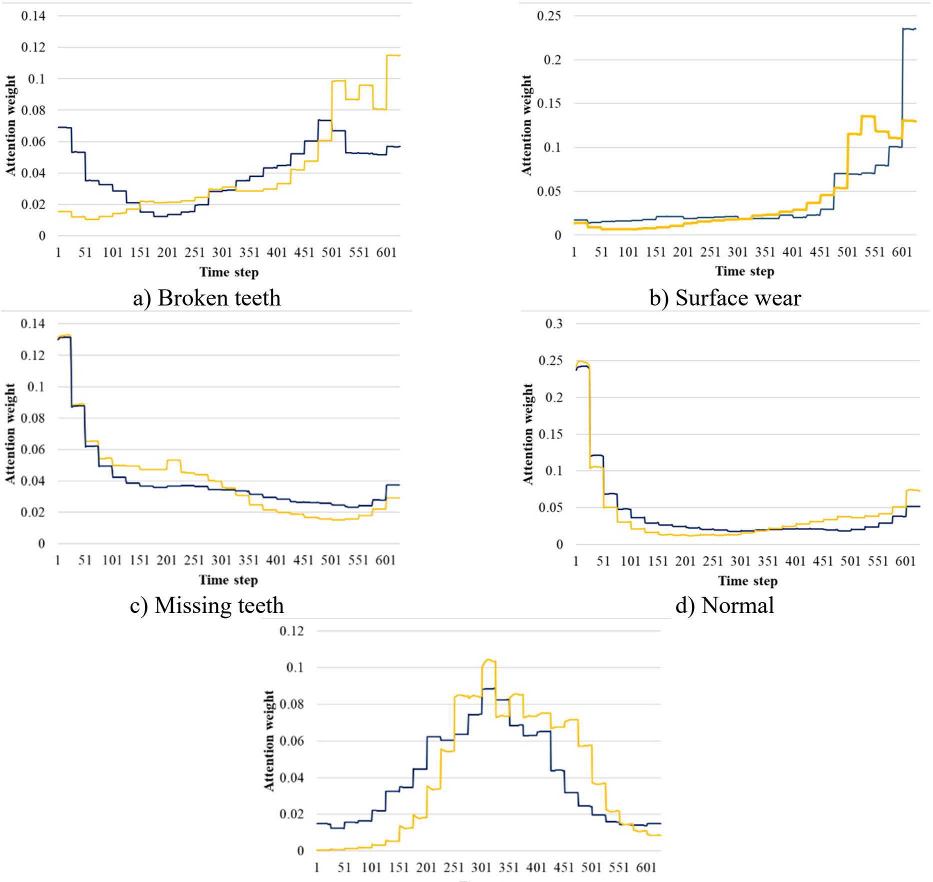

a) Broken teeth

b) Surface wear

c) Missing teeth

d) Normal

e) Root crack

Fig. 11. Attention distribution of different sun wheel health states in source domain and target domain

3.4. Model diagnosis results and analysis

The influence of AM is verified by comparing transfer fault diagnosis experiments between different loads. The radar chart shown in Fig. 13 is a comparison of the transfer accuracy of AST-JDAN and ST-JAN under different working conditions. It can be seen from the Fig. 13 that under the transfer tasks of B-A, A-B and B-D, ST-JAN and AST-JDAN have achieved high fault diagnosis accuracy, higher than 94 %. However, the fault diagnosis accuracy of ST-JAN in the transfer tasks of A-C, A-D, B-C, C-A, C-B, C-D is significantly lower than that of AST-JDAN. The reason is that the AM can enable the model to enhance the significance of the features that are beneficial to the transfer task, making it easier for the classifier to diagnose faults. Secondly, AST-JDAN integrates domain countermeasure method in ST-JAN domain adaptation method, which enables feature generator to better extract domain invariant features.

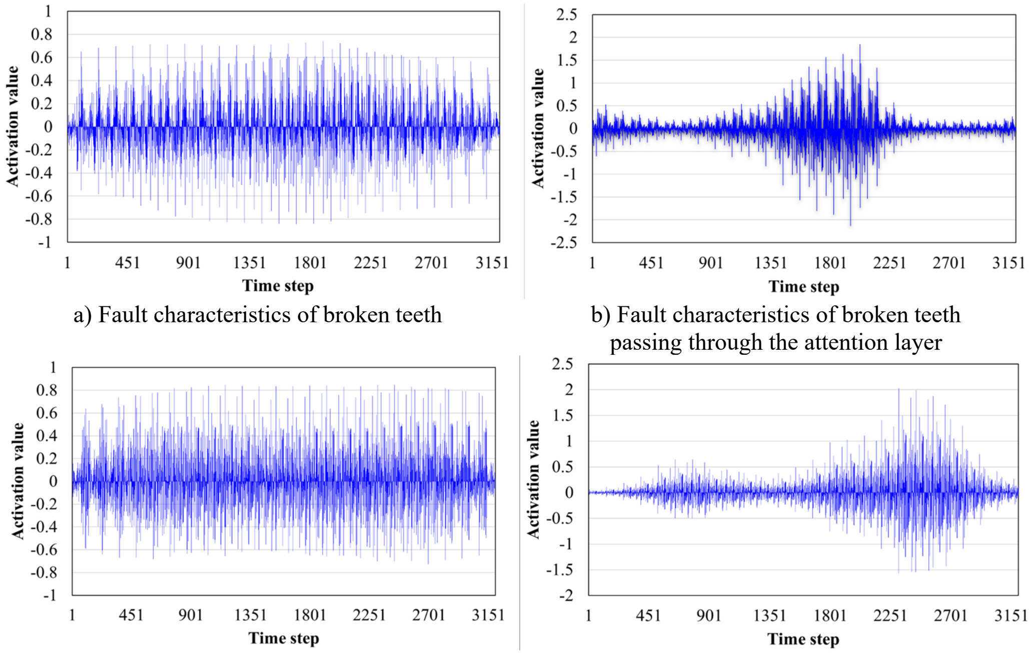

a) Fault characteristics of broken teeth

b) Fault characteristics of broken teeth passing through the attention layer

c) Fault characteristics of crack

d) Fault characteristics of crack passing through the attention layer

Fig. 12. Change diagram of fault characteristics of broken teeth and cracks in the target domain

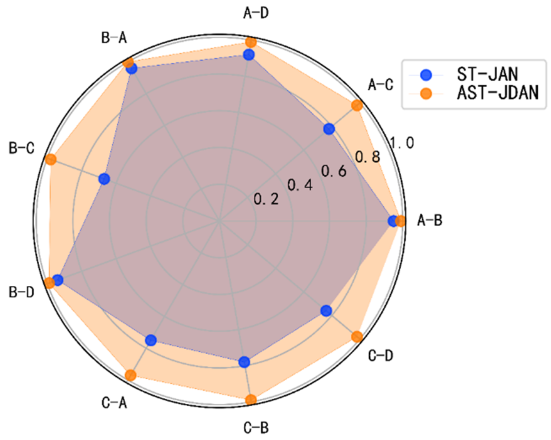

Fig. 13. Transfer diagnosis accuracy of ST-JAN and AST-JDAN under different loads

Fig. 14 shows the comparison of fault diagnosis accuracy between ST-JDAN without AM and AST-JDAN with AM under different noise intensities in transfer tasks A-B. It can be seen from the experimental data that the average fault diagnosis accuracy of AST-JDAN is about 3 %-4 % higher than that of ST-JDAN in the case of high noise intensity, but the average fault diagnosis accuracy of AST-JDAN is not significantly improved in the case of low noise intensity. The experimental results show that the AM can enable the model to extract more significant fault features, and improve the problem that features are not obvious due to the submergence of features under strong noise.

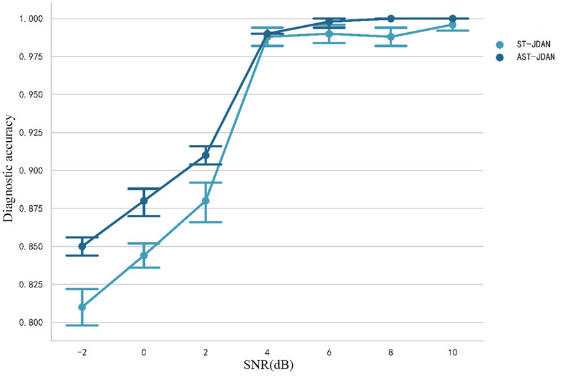

Fig. 14. Precision comparison between ST-JAN and AST-JDAN under different signal-to-noise ratios

4. Conclusions

In this paper, AST-JDAN is established. This model solves the problem of domain offset through fusion domain adaptation and domain confrontation methods. Model compression technology reduces the complexity of the model and improves the computational efficiency. The validity of the proposed model is verified by the vibration signal data set of the planetary gearbox. The results suggest that the model can obtain higher fault diagnosis accuracy in cross domain fault diagnosis, and the model has higher diagnosis accuracy than other models under strong noise interference.

This article is dedicated to the fault diagnosis of rotating machinery using deep transfer learning under variable operating conditions, but its diagnostic effectiveness depends on a large amount of annotated fault data. If fault data is scarce, the diagnostic accuracy will be greatly affected. In recent years, digital twin technology has developed rapidly. Through digital twin technology, fault data of mechanical equipment to be diagnosed can be obtained, providing a solution to the problem of scarce fault data. In the future, we will further research fault diagnosis methods that combine digital twin technology with transfer learning.

Acknowledgements

This paper was supported by the following research projects: the Key Technology Innovation Project of Fujian Province (Grant no. 2022G02030), the Natural Science Foundation of Fujian Province (Grants no. 2022J011223), and Youth and the collaborative innovation center project of Ningde Normal University (Grant No. 2023ZX01).

Data availability

The datasets generated during and/or analyzed during the current study are available from the corresponding author on reasonable request.

Author contributions

Conceptualization, Mengmeng Song and Shungen Xiao; software, Zexiong Zhang; validation, Mengwei Li, Jihua Ren and Yaohong Tang; writing-original draft preparation, Zexiong Zhang; writing-review and editing, Zicheng Xiong.

Conflict of interest

The authors declare that they have no conflict of interest.

References

[1] Z. Li, S.-S. Zhong, and L. Lin, "Novel gas turbine fault diagnosis method based on performance deviation model," *Journal of Propulsion and Power*, Vol. 33, No. 3, pp. 730–739, May 2017, https://doi.org/10.2514/1.b36267

[2] C. M. Vong and P. K. Wong, "Engine ignition signal diagnosis with wavelet packet transform and multi-class least squares support vector machines," *Expert Systems with Applications*, Vol. 38, No. 7, pp. 8563–8570, Jul. 2011, https://doi.org/10.1016/j.eswa.2011.01.058

[3] Y. Li, B. Miao, W. Zhang, P. Chen, J. Liu, and X. Jiang, "Refined composite multiscale fuzzy entropy: Localized defect detection of rolling element bearing," *Journal of Mechanical Science and Technology*, Vol. 33, No. 1, pp. 109–120, Jan. 2019, https://doi.org/10.1007/s12206-018-1211-8

[4] M. M. M. Islam and J.-M. Kim, "Automated bearing fault diagnosis scheme using 2D representation of wavelet packet transform and deep convolutional neural network," *Computers in Industry*, Vol. 106, pp. 142–153, Apr. 2019, https://doi.org/10.1016/j.compind.2019.01.008

[5] L. Chen, K. An, D. Huang, X. Wang, M. Xia, and S. Lu, "Noise-boosted convolutional neural network for edge-based motor fault diagnosis with limited samples," *IEEE Transactions on Industrial Informatics*, Vol. 19, No. 9, pp. 9491–9502, Sep. 2023, https://doi.org/10.1109/tii.2022.3228902

[6] Y. Liu, R. Young, and B. Jafarpour, "Long-short-term memory encoder-decoder with regularized hidden dynamics for fault detection in industrial processes," *Journal of Process Control*, Vol. 124, pp. 166–178, Apr. 2023, https://doi.org/10.1016/j.jprocont.2023.01.015

[7] H. Shao, W. Li, B. Cai, J. Wan, Y. Xiao, and S. Yan, "Dual-threshold attention-guided GAN and limited infrared thermal images for rotating machinery fault diagnosis under speed fluctuation," *IEEE Transactions on Industrial Informatics*, Vol. 19, No. 9, pp. 9933–9942, Sep. 2023, https://doi.org/10.1109/tii.2022.3232766

[8] G. Yuan, Z. Liang, Z. Jiawei, W. Bojia, and Y. Zhongchao, "Research on reliability of centrifugal compressor unit based on dynamic Bayesian network of fault tree mapping," *Journal of Mechanical Science and Technology*, Vol. 37, No. 5, pp. 2667–2677, May 2023, https://doi.org/10.1007/s12206-023-0440-7

[9] X. Yan, W. Liang, G. Zhang, B. She, and F. Tian, "Fault diagnosis method for complex feeding and ramming mechanisms based on SAE-ACGANs with unbalanced limited training data," *Journal of Vibration and Shock*, Vol. 42, No. 2, pp. 89–99, Jan. 2023.

[10] M. Demetgul, K. Yildiz, S. Taskin, I. N. Tansel, and O. Yazicioglu, "Fault diagnosis on material handling system using feature selection and data mining techniques," *Measurement*, Vol. 55, pp. 15–24, Sep. 2014, https://doi.org/10.1016/j.measurement.2014.04.037

[11] W. Zhang, X. Li, X.-D. Jia, H. Ma, Z. Luo, and X. Li, "Machinery fault diagnosis with imbalanced data using deep generative adversarial networks," *Measurement*, Vol. 152, p. 107377, Feb. 2020, https://doi.org/10.1016/j.measurement.2019.107377

[12] D. Zhao, S. Liu, H. Du, L. Wang, and Z. Miao, "Deep branch attention network and extreme multi-scale entropy based single vibration signal-driven variable speed fault diagnosis scheme for rolling bearing," *Advanced Engineering Informatics*, Vol. 55, p. 101844, Jan. 2023, https://doi.org/10.1016/j.aei.2022.101844

[13] K. Weiss, T. M. Khoshgoftaar, and D. Wang, "A survey of transfer learning," *Journal of Big Data*, Vol. 3, No. 1, pp. 1–40, Dec. 2016, https://doi.org/10.1186/s40537-016-0043-6

[14] T. Han, C. Liu, W. Yang, and D. Jiang, "A novel adversarial learning framework in deep convolutional neural network for intelligent diagnosis of mechanical faults," *Knowledge-Based Systems*, Vol. 165, pp. 474–487, Feb. 2019, https://doi.org/10.1016/j.knosys.2018.12.019

[15] Y. Xu, Y. Sun, X. Liu, and Y. Zheng, "A digital-twin-assisted fault diagnosis using deep transfer learning," *IEEE Access*, Vol. 7, pp. 19990–19999, 2019, https://doi.org/10.1109/access.2018.2890566

[16] Y. Cheng, D. Wang, P. Zhou, and T. Zhang, "Model compression and acceleration for deep neural networks: The principles, progress, and challenges," *IEEE Signal Processing Magazine*, Vol. 35, No. 1, pp. 126–136, Jan. 2018, https://doi.org/10.1109/msp.2017.2765695

[17] M.-H. Guo et al., "Attention mechanisms in computer vision: A survey," *Computational Visual Media*, Vol. 8, No. 3, pp. 331–368, Sep. 2022, https://doi.org/10.1007/s41095-022-0271-y

[18] J.-H. Kim, J. Jun, and B.-T. Zhang, "Bilinear attention networks," *arXiv:1805.07932v2*, 2018, https://doi.org/10.48550/arxiv.1805.07932

[19] C. Wu, F. Wu, T. Qi, Y. Huang, and X. Xie, "Fastformer: Additive attention can be all you need," *arXiv:2108.09084*, 2021, https://doi.org/10.48550/arxiv.2108.09084

[20] Y. Ganin et al., “Domain-adversarial training of neural networks,” *arXiv.1505.07818*, 2015, https://doi.org/10.48550/arxiv.1505.07818

[21] A. G. Howard et al., “Mobilenets: Efficient convolutional neural networks for mobile vision applications,” *arXiv:1704.04861*, 2017, https://doi.org/10.48550/arxiv.1704.04861

[22] L. Luo, T. Zhu, G. Zhang, Q. Ding, and Z. Huang, “Building extraction from high-resolution remote sensing images based on deeplabv3+ model,” *Electronic Information Countermeasure Technology*, Vol. 36, No. 4, pp. 65–69, 2021.

[23] K. Han, Y. Wang, Q. Tian, J. Guo, C. Xu, and C. Xu, “Ghostnet: More features from cheap operations,” in *Proceedings of the IEEE/CVF conference on computer vision and pattern recognition*, pp. 1580–1589, 2019, https://doi.org/10.48550/arxiv.1911.11907

[24] M. Song, Z. Zhang, S. Xiao, Z. Xiong, and M. Li, “Bearing fault diagnosis method using a spatio-temporal neural network based on feature transfer learning,” *Measurement Science and Technology*, Vol. 34, No. 1, p. 015119, Jan. 2023, https://doi.org/10.1088/1361-6501/ac9078

Mengmeng Song is an associate professor at Ningde Normal University in Fujiang, China. She received Master in School of Mechanical Engineering from Jiangxi University of Science and Technology, Jiangxi, China, in 2012. Now she works at Ningde Normal University. Her current research interests include signal processing and fault diagnosis. she has charged of about 11 important scientific research projects, and published about 18 papers in journals.

Zicheng Xiong is a postgraduate at Fuzhou University in Fujian, China. He received bachelor’s degree from Wuhan University of science and technology, Hubei, China, in 2019. His current research interests include fault diagnosis and deep learning.

Zexiong Zhang is a postgraduate at Fujian Agriculture and Forestry University in Fujian, China. He received bachelor’s degree from Nanchang Aviation University, Jiangxi, China, in 2019. His current research interests include AUTOSAR developing, fault diagnosis and deep learning.

Jihua Ren is a senior engineer and director in DongGuan XingHuo gear Ltd. He got a Ph.D. from Beijing University of Technology, Beijing, China in 2021. His current research interests include gear design and gear manufacture. He has charged of about 20 important scientific research projects.

Mengwei Li is a postgraduate at Fujian Agriculture and Forestry University in Fujian, China. He received bachelor’s degree from University of Jinan, Shandong, China, in 2020. His current research interests include eddy current test.

Shungen Xiao is a Professor at Fuzhou University and Ningde Normal University in Fujiang, China. He received the Ph.D. degree from Shanghai University, Shanghai, China, in 2019. His current research interests include fault diagnosis and nonlinear dynamics. He has charged of about 23 important scientific research projects, and published about 40 papers in journals.

Yaohong Tang e is a Professor at Ningde Normal University in Fujiang, China. He received Master from Tianjin University, Tianjin, China, in 2005. His current research interests include mechanical symmetry, CAx integration and fault diagnosis. He has charged of about 10 important scientific research projects, and published about 26 papers in journals.